International Journal of Thermofluids 10 (2021) 100093

Contents lists available at ScienceDirect

International Journal of Thermofluids

journal homepage: www.elsevier.com/locate/ijtf

Application to micro-cogeneration of an innovative dual fuel compression ignition engine running on biogas

Francesco Legrottaglie, Enrico Mattarelli, Carlo Alberto Rinaldini, Francesco Scrignoli*

Dipartimento di Ingegneria "Enzo Ferrari", Università degli Studi di Modena e Reggio Emilia, via Pietro Vivarelli 10, Modena 41125, Italy

ARTICLE INFO

Article History:
Received 28 November 2020
Revised 26 March 2021
Accepted 17 April 2021
Available online 26 April 2021

Keywords:
Biogas
CFD
Cogeneration
Light duty diesel engine
Natural gas
RCCI

ABSTRACT

Renewable sources and enhancement of energy conversion efficiency are the main paths chosen by the European Community to stop climate changes and environmental degradation, and to enable a sustainable growth. For this purpose, the construction of a new and more dynamic electricity distribution network is mandatory. This "smart grid" should also include small and medium-size companies, able to program the generation and use of energy from renewable sources (the so-called "prosumers"). In this frame, micro-cogeneration (rated electric power up to 50 kW) is one of the most promising techniques.

In this work, the application to micro-cogeneration of an innovative Compression Ignition internal combustion engine, operated in Dual Fuel mode is proposed. Thanks to the specific combustion system (Reactivity Controlled Compression Ignition, RCCI: a lean homogenous mixture of air and biomethane or biogas is ignited by the injection of a small amount of Diesel fuel), brake thermal efficiency can be increased at all operating conditions, compared to a conventional Spark Ignition engine running on biomethane or biogas. The ensuing reduction of CO_2 emissions is higher than 20%. Furthermore, the proposed engine can tolerate larger variations in the composition of the biogas, without a significant drop of thermal efficiency. Finally, in case of emergency, it is able to run on Diesel fuel only.

The use of the engine is particularly suitable for a company operating in the agricultural field, such as a mid-size farm, that is able to produce biogas for its self-consumption. Therefore, a representative study case is selected, and the corresponding electrical and thermal energy needs are analysed throughout a typical year. The energetic analysis leads to the identification of the most suitable engine size and calibration settings, in order to reduce the purchase of electricity and natural gas, maximizing the use of the company's own renewable sources (biogas or biomethane). The final goal of the optimization process is to create a virtuous system, that can reduce the environmental impact and make the company almost independent from the energetic point of view.

1. Introduction

In order to stop climate changes on our planet and enable a sustainable growth, it is necessary to reduce the carbon footprint of all the sectors of human activities, such as the production of energy, industry, transportation, agriculture, buildings, et cetera.

For instance, the efficiency of industrial processes characterized by exhaust streams (cement industry, steel, aluminium and ceramic tiles manufacturing, et cetera) can be improved by means of the recovery of waste heat and the following reuse within the industrial plant. The waste heat can be recovered by using heat pipe heat exchanger [1] or latent thermal energy storage [2] technologies. The stored thermal energy can be used for many different purposes, in both buildings and other industrial processes, or to produce electric power by means of organic Rankine cycle [3] or thermoelectric generators [4].

As far as the energy sector is concerned, a promising proposal is the implementation of a flexible and efficient energy distribution system, i.e. a "smart grid". In this scenario, micro-cogeneration (production of electrical energy and heat, up to 50 kW of electric power) is very interesting for small and medium sized companies, in particular for those able to use a self-produced renewable fuel. A typical example is a medium-sized farm, whose activities include raising cattle, cultivation of fields for feeding the animals and production of milk and cheese. Such a farm can also produce a good quality biogas from cattle manure, agricultural wastes and specific crops. Obviously, the fuel is not for sale (its production and distribution costs would be too high in comparison to conventional fuels), but it can be used to run an internal combustion engine, for the self-production of electricity and heat (micro-cogeneration). In this way, the farm can be almost completely independent from the energetic point of view, saving

* Corresponding author.
E-mail address: francesco.scrignoli@unimore.it (F. Scrignoli).

https://doi.org/10.1016/j.ijft.2021.100093

Nomenclature

ATDC	After Top Dead center
BTDC	Before Top Dead center
CA	Crank Angle
CFD	Computational Fluid Dynamics
CI	Compression Ignition
DF	Dual Fuel
DOS	Diesel Oil Surrogate
ECU	Electronic Control Unit
EGR	Exhaust Gas Recirculation
HC	Unburnt Hydrocarbons
HD	Heavy-Duty
IDI	Indirect Injection
KH-RT	Kelvin-Helmholtz Rayleigh-Taylor
ND	Normal Diesel
NDIR	NonDispersive Infrared
NG	Natural Gas
PaSR	Partially Stirred Reactor
SI	Spark Ignition
SOI	Start Of Injection
TDC	Top Dead Centre
TFC	Turbulent Flame Closure
VGT	Variable Geometry Turbine

Chemical formulae

CH_4	Methane
CO	Carbon Monoxide
CO_2	Carbon Dioxide
NO_x	Oxides of Nitrogen (NO+NO_2)
O_2	Oxigen

Subscripts and superscripts

aii	as it is
c	combustion
CO	carbon monoxide
D	Diesel fuel
dm	dry matter
lw	live weight
NG	Natural Gas
vs	volatile substance

Symbols and units

m_D	Mass of Diesel fuel provided to the engine per cycle in normal Diesel operation, mg
m_{NG}	Mass of natural gas provided to the engine per cycle in dual fuel operation, mg
m'_D	Mass of Diesel fuel provided to the engine per cycle in dual fuel operation, mg
$\dot{m}_{NG}$	Natural gas mass flow rate, g/s
$\dot{m}_{air}$	Air mass flow rate, kg/s
P_{in}	Power provided to the engine by means of fuel(s), kW
S_D	Substitution rate of the high reactivity fuel,%
X_D	Fraction of energy introduced with Diesel fuel in dual fuel mode,%
X_{NG}	Fraction of energy introduced with natural gas in dual fuel mode,%
AFR	Air to Fuel Ratio
AHRR	Apparent Heat Release Rate, J/°
BMEP	Brake Mean Effective Pressure, bar
BTE	Brake Thermal Efficiency,%
CAD	Crank Angle Degree, °
CN	Cetane Number
CO	concentration of carbon monoxide, ppm
FMEP	Friction Mean Effective Pressure, bar
HC	Concentration of methane equivalent unburnt hydrocarbons, ppm
IMEP*	gross Indicated Mean Effective Pressure, bar
LHV_{CO}	Carbon monoxide lower heating value, MJ/kg
LHV_D	Diesel fuel lower heating value, MJ/kg
LHV_{NG}	Natural Gas lower heating value, MJ/kg
PPRR	Peak Pressure Rise Rate, bar/°
RI	Ringing Intensity, MW/m^2
RoHR	Rate of Heat Release, J/°
RON	Research Octane Number
WI	Wobbe Index, MJ/Nm^3

Greek symbols

η_c	combustion efficiency,%

money while strongly reducing its carbon print, in comparison to a conventional farm.

The chemical and physical characteristics of a biogas are strongly variable, as shown in Table 1, depending on the feedstock used for its production.

In order to burn a fuel with such a different composition, a Spark Ignition (SI) engine must be equipped with a sophisticated electronic control system, able to keep regular operations and prevent knocking. The fuel conversion efficiency of this type of engines is limited by some technical aspects:

- compression ratio is low, to prevent knocking;
- combustion is usually not complete, due to the necessity of running on rich mixtures;
- when running at partial load, the engine has high throttling losses.

Passing from SI to Compression Ignition (CI), all the problems listed above can be fixed: compression ratio could be risen up considerably, combustion is always lean, and load can be controlled without throttling the flow. Biogas can be injected within the intake manifold, as on a standard SI engine, and combustion will be primed by the injection of a small quantity of Diesel fuel. This concept - referred to as Reactivity Controlled Compression Ignition (RCCI), or Dual Fuel (DF) combustion - is well assessed and investigated by several experimental and numerical studies, considering a number of different fuels [6–19]: in comparison to a SI engine delivering the same brake power, a DF engine can have a higher fuel conversion efficiency, or Brake Thermal Efficiency (BTE), so reducing the amount of CO_2 emissions.

Moreover, Molina et al. (2015) [14] demonstrated that this type of combustion concept, when applied to a conventional Diesel engine, can reduce NO_x and soot emissions simultaneously. This outcome is particularly promising, because in the standard CI combustion it is very difficult to find a good trade-off between the two types of

Table 1
Biogas features [5].

Constituents	**Range**
CH_4 [vol. fraction -%]	30 ÷ 73
CO_2 [vol. fraction -%]	20 ÷ 40
N_2 [vol. fraction -%]	5÷40
O_2 [vol. fraction -%]	0 ÷ 5
H [vol. fraction -%]	1 ÷ 3
H_2S [vol. fraction -%]	0 ÷ 0.01
Physical properties	**Values**
Density [kg/m^3]	0.65–0.91
Octane number [-]	130
Auto-ignition temperature [°C]	632–813
Lower Heating Value [MJ/Nm^3]	10 ÷ 25

pollutants (all the measures taken to reduce the former tend to make the latter increase, and vice versa). Finally, RCCI applied to Diesels may also improve BTE, thanks to a faster combustion process.

As far as the combustion rate of RCCI is concerned, it is essential to highlight its dependence on fuel stratification. In fact, as demonstrated by Liu et al. [15], local fuel reactivity and concentration strongly influence the ratio of flame front propagation and auto-ignition, and hence the combustion development. The proper fuel stratification is also important in order to induce High Temperature Heat Release (HTHR) both in high and low reactivity regions of the combustion chamber, limiting HC emissions [16].

However, as engine load increases from low to medium, the control of RCCI combustion applied Diesel engines becomes more and more difficult: cylinder pressure tends to rise abruptly, generating high peaks and gradients, which increase combustion noise and the risk of mechanical failures. Therefore, to operate at medium-high loads, high amount of Exhaust Gas Recirculation (EGR) and/or low compression ratios (CR) are needed, at the expense of BTE. Nieman et al. [11] have found that replacing gasoline with a fuel characterized by a higher octane number, such as Natural Gas (NG), is effective to extend RCCI operation to high loads with acceptable levels of Peak Pressure Rise Rate (PPRR) and Ringing Intensity (RI). In detail, they explored a wide range of loads and speeds (Indicated Mean Effective Pressure, IMEP, from 4 to 23 bar, and engine speed from 800 to 1800 rpm,) on a Heavy-Duty (HD) Diesel, maintaining the original CR (16:1). The results of the study show that RCCI NG-diesel guarantees a controllable, efficient and clean operation up to IMEP = 13.5 bar without EGR, while at higher loads the use of EGR is mandatory to reduce NO_x emissions. They also carried out a comparison between the NG-diesel and the gasoline-diesel combustion concepts, at IMEP = 9 bar. Using NG instead of gasoline permits to strongly reduce PPRR and RI (more than halved); moreover, soot emissions are reduced by more than 70%, compared to DF gasoline/diesel operations. On the other hand, the higher adiabatic flame temperature of NG determines higher temperatures within the cylinder: as a result, NO_x emissions increase while efficiency slightly decreases (due to greater wall heat transfer losses).

Moreover, Tong et al. [17] have demonstrated that it is possible to preserve stable and controllable RCCI operations up to higher loads if gasoline-polyoxymethylene dimethyl ethers (PODE) is used, instead of gasoline-diesel. In particular, the maximum load achievable with gasoline-PODE operation is IMEP=17.6 bar, versus IMEP = 13.9 bar in gasoline-diesel operation.

As far as biogas is concerned, its use as a low reactivity fuel in RCCI combustion is not a novelty. In the study presented in Ref. [5], a 4-Stroke turbo-charged Indirect Injection (IDI) Diesel engine was operated in single fuel mode (diesel and biodiesel) and DF mode (biogas-diesel and biogas-biodiesel), in order to compare combustion and emissions characteristics. The engine was run at a constant speed of 2000 rpm, at different loads (20, 40, 60, 80, 100%). In DF operations, the amount of biogas injected per cycle was kept constant, while the mass of pilot fuel was varied according to the engine load. The start of injection (SOI) of the high reactivity fuel was set at 12° before TDC, in all cases. In DF operations, with both fuel blends, NO_x emissions strongly decrease (about 70% lower), in comparison to the single fuel operations. Also soot and CO_2 emissions are lower. Conversely, the concentrations of CO and HC were found to be considerably higher than those corresponding to the single fuel operations. This outcome was expected, and the use of a specific oxidation catalyst was proposed to fix the problem. The study also shows longer combustion durations and lower pressure gradients within the cylinder, when passing from single fuel to DF mode, demonstrating that the last type of combustion is smoother than the former.

In conclusion, the above mentioned references (and many others available in literature), highlight the potential advantages of the use of NG and biogas in DF RCCI engines. However, they also show many challenges for the practical implementation of a mass production engine, starting from the optimization of the Diesel fuel injection strategy, to the control of the premixed charge. Without a proper setup, the homogeneous mixture within the cylinder may not be able to burn completely, or, in the worst case, it may explode, damaging the engine. The variation of the fuel composition is a further obstacle to engine control.

In this study, an innovative DF engine running on biogas is proposed for micro-cogeneration. The novelty consists in the smart modification (low cost, no compromise on reliability, performance and emissions) of a CI, 4-cylinder, 2.8 L turbocharged automotive engine. Differently from the majority of existing DF power plants, the “donor” is a light-duty engine, with a relatively high specific power.

The new engine is optimized for micro-cogeneration, so that the maximum electric power is 50 kW at 3000 rpm.

The development of the engine is mainly based on a comprehensive experimental campaign, carried out on another version of the DF engine, running on Diesel fuel and NG [20]. The collected experimental data are used to calibrate and validate a CFD-3D combustion model; then, this model is applied to the theoretical study of DF combustion, with different compositions of biogas. As it will be shown in the following sections, the proposed engine is able to burn almost any type of biogas in a clean and efficient way, with minor adjustments to the control strategy.

In order to assess the advantages in terms of fuel conversion efficiency and CO_2 emissions, the proposed engine is compared to a more conventional SI engine, running on biogas and having the same power output.

Finally, a financial analysis on the application of the proposed micro-cogeneration system is presented: it demonstrates that, besides the environmental aspects, the concept is convenient also from an economical point of view.

2. Energy requirements analysis

This study considers a typical medium sized agro-zootechnical company, located in Italy. In particular, it is a dairy farm, producing milk and cheese, including Parmigiano Reggiano. It owns a stable, with a herd of 180 heads. About half of these are dairy cows, while the remaining ones are non-productive [21].

The farm has got about 140 hectares of cultivated land for forage production. The typical spring-summer crops are sorghum, alfalfa and polyphite grass, while the winter crops are barley and wheat. The forage production is approximately 5825 ton_{aii}/year. As it can be noted from Table 2, sorghum and corn have the main shares of the crop, in terms of weight [22].

After mowing, the forage is compacted in the form of round bales, dried and stored in an aired barn.

The 66% of the fodder production is intended for sale, while the remaining part is used for feeding the farm's own livestock. The latter requires about 1200 ton_{dm} of crops (about 6 ton_{dm} of crops per year for each cow), corresponding to about 73 ha of the cultivated area.

Table 2
Annual production and humidity content of crops, and thermal energy required for drying.

Crops	Annual production [ton_{aii}/year]	Moisture [%]	Thermal energy required for drying [kWh]
Chopped corn	1850	45	348,000
Winter grain silage (barley, wheat, triticale)	420	40	107,000
Forage sorghum	2450	40	678,000
Alfalfa	445	56	202,000
Permanent lawn	660	65	365,000

The cereal production is stored within silos (500 ton_{aii} for corn and 370 ton_{aii} for sorghum), and it's grinded into flour before feeding the animals.

It's important to notice that the self-production of the forage is a mandatory requirement for obtaining the bio denomination of the milk and to comply with the Production Regulation of Parmigiano Reggiano cheese.

The main production processes of the farm are listed in the following.

- Crop drying: crop humidity must be lowered to a value of 15%. The process absorbs a considerable amount of thermal energy, since it takes place for about 200 days per year, 16 h per day, and it consists in a slow water vaporization at relatively low temperatures.
- Milking: the annual production of milk is between 8000 and 9000 quintals, on average 25 litres per day for each head during the lactation period [21]. The milking of the cows, as well as the milk storage and processing need both thermal and electrical energy.

2.1. Thermal users

Table 3 presents the main thermal users of the farm. For the sake of brevity, the calculations are not presented in this section, but they can be found in Table A1, moved to the Appendix.

The profiles of thermal power demand of a typical day, in both winter and summer, are reported in Figs. 1 and 2: the first graph refers to the period when the crop drying process is active, while the second presents the demand throughout the remaining 156 days of the year.

Table 3
Main thermal users of the farm.

Utilities	Thermal power [kW]
Crop drying	530
Heating and domestic water	25
Cheese production and milk pasteurization	37

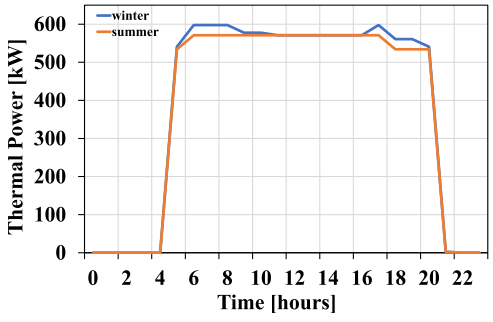

Fig. 1. Thermal power demand of the farm with crop drying process.

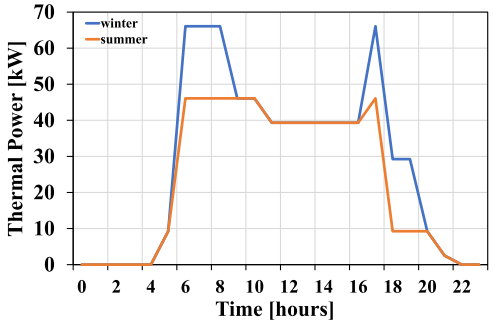

Fig. 2. Thermal power demand of the farm without crop drying process.

Table 4
Main electrical utilities of the farm.

Users	Electric power [kW]
Dryer ancillaries	12
Grain grinding	10
Mixer	3
Feeders	6
Well pump	3
Stable ventilation and milking	6.75
Manure ramp	3
Waste collection	3
Waste separation	2.2
Lighting	2.6
Cheese production	10
Washing - cleaning	3
Circulation pumps	2
Manure treatment for fertilization	8
Milk storage	11
Milk shaker	3.5

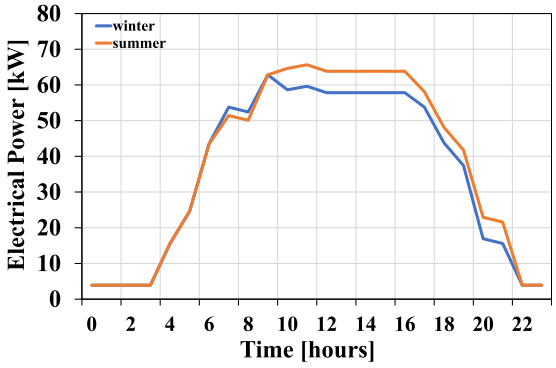

Fig. 3. Electrical power demand of the farm.

2.2. Electrical users

The farm has a maximum electrical supply of 100 kW, that fully covers its production needs. The main electrical users are reported in Table 4. For further details, the reader can refer to Table A2 in the Appendix.

The resulting electrical power demand profiles of a typical day, in both winter and summer, are shown in Fig. 3.

3. The reference engine

On the basis of the analyses presented in the previous section, the engine selected for this study is an automotive 4-cylinder turbocharged Diesel engine, manufactured by VM Motori (Cento, Italy). The main engine features are listed in Table 5.

Table 5
Main parameters of the reference engine.

Engine Type	HSDI 4-S Diesel, EURO IV
Cylinders	4 in-line
Total displacement [L]	2.78
Bore x Stroke [mm]	94×100
Compression ratio	17.5:1
# of valves per cylinder	4
Air Metering	VGT + Intercooler
Injection system	Common Rail
Max. Injection press. [MPa]	160
Injector hole diameter [mm]	0.153
Number of injector holes	6
EGR system	High Pressure, cooler, throttle
Max. brake power [kW@rpm]	130@3800
Max. brake torque [Nm@rpm]	440@1750
Max. Peak Cylinder pressure [bar]	150
Max. Engine Speed [rpm]	4600

The engine was fully characterized by experiments, in the original version shown in Table 5, as well as in a DF configuration, using CNG as a low reactivity fuel. The experimental campaign also included the calibration of the engine control system. The experimental results supported the construction and calibration of accurate CFD-3D numerical models, used as the main investigation tools.

4. The experimental facility

The experimental study is performed at a dynamometer test bench featuring an eddy-current brake (Apicom FR 400 BRP: maximum power 260 kW, maximum torque 900 Nm, maximum rotational speed: 12,000 rpm) and the Apicom Horus software for system control and data acquisition. The test bench also includes two closed-loop controls: the former is applied to the eddy-current brake in order to control the revolution speed, the latter to the engine accelerator pedal, in order to control the torque output.

The laboratory instrumentation, besides the standard pressure and temperature transducers, includes a Coriolis flow meter and the Alicat MCE gas mass flow controller for measuring the Diesel fuel and the NG consumption, respectively. The airflow rate is measured by means of a hot wire anemometer. A high frequency indicating system has been used. It is made up of a Kistler 6058A piezo-electric transducer (installed on one cylinder in place of the glow plug), a charge amplifier, an encoder with FIA-F light barrier by Sensor Instruments, the National Instruments CompactRIO system and the combustion analysis software OBI by Alma Automotive. It permits to acquire, with an angular resolution of 0.1°, in-cylinder pressure trace and calculate the related parameters in real time, for combustion monitoring. At each investigated operating point, 100 consecutive engine cycles are sampled for the evaluation of the ensemble average in-cylinder pressure trace, which is used for offline calculations. The optimization of the engine control parameters is supported by the ETAS INCA software and an ECU equipped with an ETK module. In order to measure the gaseous emissions of the engine, the MRU VARIOplus Industrial has been used. In particular, the device detects the following gaseous emissions:

- CO, CO_2 and CH_4, using Nondispersive Infrared (NDIR) modules;
- O_2, NO_x ($NO+NO_2$), using electrochemical sensors.

Meanwhile, soot emissions have been measured thanks to the AVL DiSmoke 4000 opacimeter. It is important to note that all the measured pollutants concentrations are raw, since the aftertreatment system is not installed. Finally, the actuation signal of a Diesel injector, together with the optical encoder signal, have been acquired by using an oscilloscope, in order to evaluate timing and duration of each shot.

In order to implement a DF NG-Diesel combustion system on the reference engine, it is equipped with four NG injectors, with a nominal flow rate of 1.5 g/s at 3 bar, installed on the engine inlet pipe, just downstream of the intercooler and about 500 mm before the intake plenum. Such a solution permits to improve air-NG mixing and guarantees a more uniform distribution of the charge amongst the cylinders. The NG injectors are controlled by means of a specific ECU, that requires the following main input signals: engine rotational speed, engine load, intake pressure and temperature, exhaust gas temperature.

Table 6 reports the main physical and chemical properties of NG and Diesel fuel employed during the experimental study. As far as the NG composition is concerned, methane represents the 95% in volume.

5. Engine calibration

Despite the peak of electrical power demand of the farm is about 65 kW_e (see Fig. 3), it has been chosen to limit the maximum electrical power deliverable by the engine to 50 kW_e. In this way, it is possible to remain in the frame of micro-cogeneration and to take benefit from simplified administrative and authorization procedures. Moreover, this choice permits to exploit almost all the self-production of electrical and thermal energy.

Table 6
Properties of NG and diesel fuel, employed in the study.

Fuel properties	NG	Diesel fuel
Lower heating value (LHV) [MJ/kg]	49	43.5
Stoichiometric air-fuel ratio	17.0	14.5
Heating value of stoichiometric mixture [MJ/kg]	2.72	2.81
Research Octane Number (RON)	≈ 120	–
Cetane Number (CN)	–	52
Autoignition temperature [°C]	650	200

Assuming a 90% efficiency of the alternator coupled to the engine crankshaft the above-mentioned electrical power limit corresponds to a mechanical power of 55.5 kW.

In order to guarantee the network frequency in Europe (50 Hz), two solutions are possible:

- engine revolution speed: 1500 rpm; 4-pole alternator;
- engine revolution speed: 3000 rpm; 2-pole alternator.

The latter solution is more attractive than the first one since a 2-pole alternator is more compact and less expensive. It should be noted that, differently from the case of HD engines, the engine speed falls well below its maximum limit (4600 rpm).

Therefore, the full load operating point considered in this study is 3000 rpm-177 Nm/8 bar BMEP (corresponding to 55.5 kW).

During the tests, the transition from Normal Diesel (ND) to DF operation is obtained by progressively replacing Diesel fuel with NG. The closed-loop control applied to the engine pedal keeps the brake torque constant, without any modification to the original Diesel engine set-up. Only in a second phase, the Diesel fuel injection strategy has been optimized.

In order to guarantee the repeatability of the tests, particular care has been devoted to maintaining as constant as possible the operating conditions, in particular engine speed, brake torque, boost pressure, oil and coolant temperature. Moreover, during the tests, the EGR valve is kept always shut. Therefore, the influence of charge dilution with exhaust gas was not considered.

At the full load operating point considered in this study (3000 rpm-8 bar BMEP), it is possible to replace the 80% of Diesel fuel with NG, maintaining the same torque output and regular engine operations. The substitution rate of the high reactivity fuel (S_D), is expressed by the following formula:

$$S_D[\%] = X_D[\%] - 100 = \left(\frac{m_D'}{m_D} - 1\right)100 \quad (1)$$

where $X_D = \frac{m_D'}{m_D}$ is the ratio of the mass of Diesel fuel injected in DF condition, m_D', to the mass of Diesel fuel injected in ND condition, m_D.

The fraction of fuel energy associated to NG, entering the combustion chamber can be expressed as:

$$X_{NG}[\%] = \left(\frac{m_{NG}.LHV_{NG}}{m_D.LHV_D}\right)100 \quad (2)$$

m_{NG} is the mass of NG injected per cycle in DF mode; LHV_{NG} is the Lower Heating Value of NG; LHV_D is the Lower Heating Value of Diesel fuel.

At the operating point considered in the study, the energy associated to NG entering the combustion chamber is (before the calibration) 93% of the total one entering in ND mode.

In the following, the DF cases are identified by substitution rate, S_D[%] and the percentage of introduced NG energy X_{NG}[%] (as an example: "−80% *D* + 93% NG").

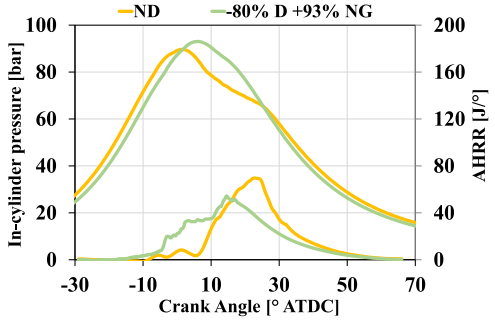

Fig. 4. Comparison between ND and DF operation in terms of in-cylinder pressure and AHRR at 3000 rpm - BMEP=8 bar. DF case is not optimized.

Fig. 4 shows the effects of the transition from ND to DF combustion mode on in-cylinder pressure trace and Apparent Heat Release Rate (AHRR). The last parameter is defined as the difference between the energy rate released by combustion and the heat rate lost through the combustion chamber walls. AHRR can be calculated from the measured in-cylinder pressure, applying the first Law of Thermodynamics to a constant mass of ideal gas, without any hypothesis on heat transfer. In order to simplify the analysis, the ratio of specific heats at constant pressure and constant volume is kept constant throughout the engine cycle (=1.3).

Looking at the AHRR curve related to ND combustion, it is possible to observe the presence of three peaks. The first two peaks are related to the premixed combustion of the small amount of Diesel fuel injected in the second half of the compression stroke (pilot and pre injections). The third peak corresponds to the main injection, whose fuel is burnt in diffusive mode. Passing from ND to DF operation, the first two peaks of AHRR increase, at the expense of the third one (in fact, the integral of the AHRR curve is about constant, representing the useful amount of heat released by combustion). The rising of the first two peaks is easily explained by the fact that the pilot and the pre injection of Diesel fuel also ignite part of the NG that surrounds the Diesel fuel jets.

Since the maximum peak of AHRR tends to be lower in DF combustion mode, also the maximum in-cylinder pressure gradient and the associated combustion noise are expected to reduce.

As far as the pressure traces are concerned, the DF case shows a higher in-cylinder pressure peak compared to ND, due to the larger advance of start of combustion. This behaviour is clearer observing the plots of cumulative apparent heat release (Fig. 5): the angle at which half of the energy is released shifts from 22.6° ATDC (ND case) to 16.4° ATDC (DF case).

Another aspect shown in Fig. 4 is the reduction of pressure during compression in DF mode, despite the identical values of boost pressure compared to ND operation. This outcome may be explained by the higher heat capacity of the air-NG mixture, in comparison to pure

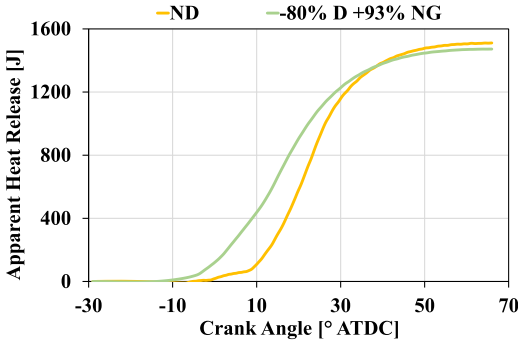

Fig. 5. Comparison between ND and DF operations in terms of apparent heat release at 3000 rpm - BMEP=8 bar. DF case is not optimized.

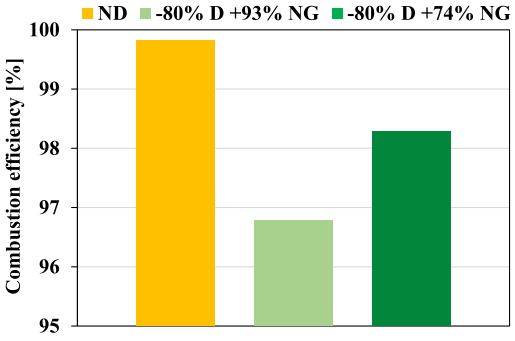

Fig. 6. Comparison between ND and DF operations in terms of combustion efficiency at 3000 rpm - BMEP=8 bar. Only "−80% *D* + 74% NG" DF case is optimized.

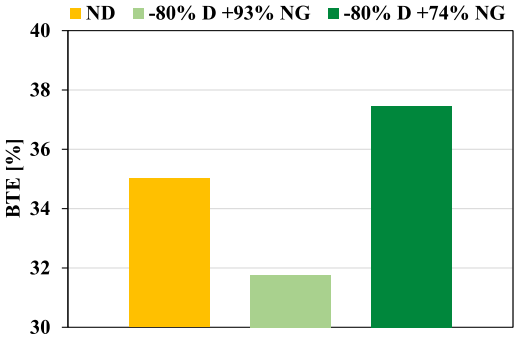

Fig. 7. Comparison between ND and DF operations in terms of BTE at 3000 rpm - BMEP=8 bar. Only "−80% *D* + 74% NG" DF case is optimized.

air, and the ensuing reduction of the polytropic index. Moreover, NG density is lower than that of air.

Figs. 6–8 present a comparison between ND and DF operations in terms of combustion efficiency, brake thermal efficiency (BTE), gaseous emissions and soot. A further DF case is included (−80% *D* + 74% NG), which derives from the optimization of the "−80% *D* + 93% NG" DF case.

Combustion efficiency (η_c) has been evaluated according to the following formula:

$$\eta_c = \frac{\left(P_{in} - \frac{HC}{10^6}\cdot\frac{16}{29}\cdot\dot{m}_{air}.LHV_{NG}.10^3 - \frac{CO}{10^6}\cdot\frac{28}{29}\cdot\dot{m}_{air}.LHV_{CO}.10^3\right)}{P_{in}}.100 \quad (3)$$

where $P_{in} = \dot{m}_{NG}.LHV_{NG} + \dot{m}_D.LHV_D$ is the power introduced with NG and Diesel fuel, in kW; $\dot{m}_{NG}$ is the NG mass flow rate, in g/s; LHV_{NG} is the Lower Heating Value of NG, in MJ/kg; $\dot{m}_D$ is the Diesel fuel mass flow rate, in g/s; LHV_D is the Lower Heating Value of Diesel fuel, in MJ/kg; *HC* is the concentration of methane-equivalent unburnt hydrocarbons, in ppm; $\frac{16}{29}$ is the ratio between the molar mass of methane and standard air; $\dot{m}_{air}$ is the air mass flow rate delivered by the engine, in kg/s; *CO* is the concentration of Carbon Monoxide, in ppm; $\frac{28}{29}$ is the ratio between the molar mass of carbon monoxide and standard air; LHV_{CO} is the Lower Heating Value of CO, in MJ/kg.

Eq. (3) does not include the contribution of hydrogen, that could not be measured during the tests. However, such an equation should provide reliable indications, at least in relative terms.

Fig. 6 clearly shows a worsening of combustion efficiency passing from ND mode to "−80% *D* + 93% NG" DF case (η_c decreases from 99.8% to 96.8%, respectively).

However, optimization permits to recover some efficiency (η_c improves from 96.8% to 98.3%). In particular, this enhancement has been obtained by increasing both rail pressure and the SOI advance of Diesel fuel injection, and also decreasing the boost

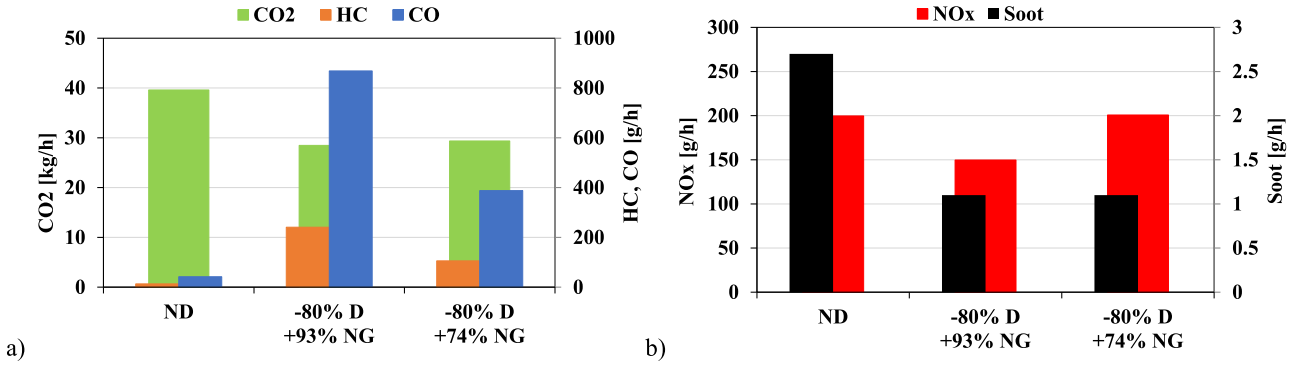

Fig. 8. Comparison between ND and DF operations in terms of CO_2, CO, HC, NO_x and soot emissions.

Table 7
Review of the calibration parameters.

DF cases	SOI[CA °BTDC]	Rail pressure [bar]	Boost pressure [bar]
−80% *D* + 93% NG	1.0	750	1.8
−80% *D* + 74% NG	6.0	1050	1.4

pressure (see Table 7). The higher injection pressure, along with the advanced injection timing, promote Diesel fuel atomization and mixing. As a consequence, Diesel fuel tends to burn more quickly, involving a larger portion of NG-air mixture. The ensuing higher rise of temperature helps the propagation of the flame front in the premixed charge from the hot spots generated by the Diesel fuel auto-ignition toward the far end of the chamber.

Fig. 7 shows that also BTE decreases in DF mode, without a specific calibration. However, thanks to the optimization of the injection strategy, the "−80% *D* + 74% NG" DF case is characterized by a higher BTE (37.5%) compared to ND operation (35%), despite the slightly lower combustion efficiency. This outcome is explained by the improvement of the thermodynamic efficiency of the optimized DF cycle, compensating the less complete combustion.

Fig. 8a highlights a relevant increase (at least one order of magnitude) of CO and HC emissions when switching from ND to "−80% *D* + 93% NG". This outcome is related to the worsening of combustion efficiency, and it can be explained by the very low speed that characterizes the flame front propagating in a homogeneous and lean NG-air mixture, as found by many researchers (as an example, by Cameretti et al. [23]). Moreover, the amount of Diesel fuel injected in DF mode is modest. Therefore, the energy released by the auto-ignition of the high reactivity fuel is relatively small, in comparison to the mass of lean NG-air mixture, making its ignition more difficult. In Fig. 8a it is also possible to observe an improvement of CO_2 emissions, mainly due to the higher H/C of methane in comparison to Diesel fuel. In detail, passing from ND to "−80% *D* + 74% NG" DF case, CO_2 emissions decrease by about 30%.

Fig. 8b shows that in the "−80% *D* + 93% NG" DF case, NO_x emissions are lower than in ND operation (NO_x emissions reduction: 25%). This is due to the reduction of the third peak of AHRR (see Fig. 4), that permits to lower the in-cylinder maximum temperature, and hence the formation of NO_x. However, in the optimized DF case ("−80% *D* + 74% NG"), NO_x emissions are comparable to the ND value, since the reduction of the maximum peak of AHRR is compensated by the increase of the main injection advance defined during the calibration process. As far as soot is concerned, Fig. 8b highlights a reduction of such an emission passing from ND to DF cases. In particular, soot emissions drop from 2.7 g/h to about 1.1 g/h, respectively. The reason of this experimental evidence is that the production of soot from diffusive combustion of liquid Diesel fuel tends to reduce, as the amount of the high reactivity fuel decreases. Moreover, Diesel fuel ignition delay time increases, due to the competition between Diesel fuel and NG for the oxygen: as a result, vaporization and mixing of the Diesel fuel droplets are enhanced. Moreover, NG does not contain PAH, and their formation in the NG flame mainly comes from the intermediate products (in particular, C_2H_2 and C_2H_5) of the oxidation of ethane and propane, which usually represent a very small fraction of NG.

Finally, Fig. 9a illustrates the correlation between AHRR and in-cylinder pressure traces; Fig. 9b presents the curves of cumulative apparent heat release; Fig. 9c compares the standard and the optimized injection strategy.

6. Sensitivity to biogas composition

In order to assess the impact of the biogas composition on the DF combustion process, a set of 3-Dimensional Computational Fluid Dynamics (3D-CFD) simulations have been carried out.

Nowadays, the CFD-3D approach represents a fundamental tool to get a deeper insight of the phenomena which take place inside of an internal combustion engine, such as the gas exchange process, mixture formation, combustion, pollutant formation, heat transfer losses, etc. Due to its versatility, the CFD approach is also largely employed to analyse and/or predict the thermo-fluid dynamics behaviour of other machines, different from internal combustion engine, such as pumps [24], and of industrial processes involving fluids [25].

The CFD-3D tool used in this work is a customized version of the KIVA-3 V code [26]. The code solves the conservation equations for evaporating fuel sprays, coupled with the CFD-3D of compressible, multi-component, reactive gases in an engine cylinder with arbitrarily-shaped piston geometry. In order to improve the accuracy of CI engine simulations, different sub-models were previously implemented by the authors in the framework of the KIVA-3 V code. In details, for modelling the breakup phase of Diesel oil, the Hybrid Kelvin-Helmholtz Rayleigh-Taylor (KH-RT) has been introduced [27], while DF combustion is obtained with two coupled modes: the "conventional" partially premixed reactor spray combustion mode, PaSR, and the flame propagation mode [28−30]. The development and validation of the chemical kinetic mechanisms for natural gas/Diesel oil compositions were carried out according to measurements of ignition delay times in shock tube experiments and flame propagation data for constituent components of natural gas; the SENKIN code was used to calculate ignition delay times under constant volume conditions [31,32]. The base natural gas is defined by a mixture of methane (≈ 96%), ethane, propane and nitrogen, whereas Diesel oil is represented by the Diesel Oil Surrogate (DOS) model, in which liquid fuel properties are the same of real diesel oil, while fuel vapour is made up of a blend of n-heptane and toluene [28]. Finally, the combustion mechanism for natural gas/Diesel oil mixture includes 81 species and 421 reactions.

These sub-models were previously implemented by the authors in the framework of the KIVA-3 V code and they are fully described in previous papers [27−32]. Moreover, the customized KIVA-3 V code

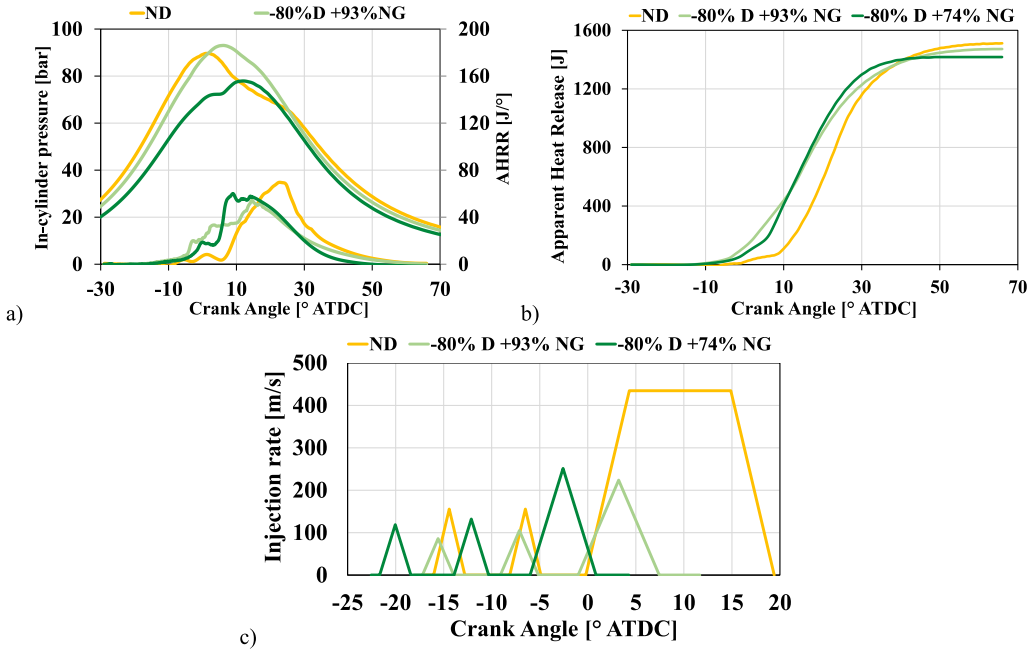

Fig. 9. Influence of Diesel fuel injection optimization (plot c) in terms of in-cylinder pressure and apparent heat release.

Table 8
Main features of fuels.

Composition [vol%]		NG	CH_4	BG50	BG65	BG75
	N_2	1.0%	0.0%	0.0%	0.0%	0.0%
	CH_4	96.0%	100.0%	50.0%	65.0%	75.0%
	C_2H_6	2.5%	0.0%	0.0%	0.0%	0.0%
	C_3H_8	0.5%	0.0%	0.0%	0.0%	0.0%
	CO_2	0.0%	0.0%	50.0%	35.0%	25.0%
Density	kg/m^3	0.694	0.668	1.255	1.079	0.962
LHV	MJ/kg	49.00	50.00	13.31	20.12	26.05
LHV	MJ/Nm^3	34.00	33.40	16.70	21.71	25.05
Wobbe Index	MJ/Nm^3	44.71	44.76	16.33	22.89	27.98

has been already applied by authors to the analysis of some Diesel [28,30,33] and DF engines [32,34,35] and the results of calculations were found in very good agreement with experiments. In particular, [35] reports the building and the experimental validation of a KIVA model of the engine considered in the current study. As shown in the paper, the CFD model is able to correctly reproduce the DF combustion process, resulting in a very accurate prediction of average cylinder pressure and RoHR, as well as exhaust gas composition. The same model presented in [35] has been used here to simulate the operating point of the current study (3000 rpm, 177 Nm / 55.5 kW). First, simulations have been performed considering the same low reactivity fuel used in [35], i.e. NG made up of methane (96%), ethane, propane and nitrogen; then, pure methane (CH_4) and 3 different compositions of biogas have been tested (BG50, BG65, and BG75). Table 8 reports the main features of the 5 different mixtures used as low reactivity fuels. All the simulations have been carried out starting from the same initial physical conditions (in-cylinder pressure, temperature, turbulent kinetic energy, turbulence length scale and swirl ratio) obtained from a combination of experimental measurements, specific CFD-1D simulations and previous CFD-3D simulations, as reported in [35].

In the current study, the initial composition has been calculated for each case, in order to keep constant the amount of energy provided by the premixed fuel. It should be noted that the initial compositions for the NG and the CH_4 cases are almost identical. Moreover, for the biogas cases, the presence of CO_2 reduces the space available for fresh air, resulting in a slightly lower air-to-fuel ratio (the amount of CH_4 is the same for all the cases, except the first).

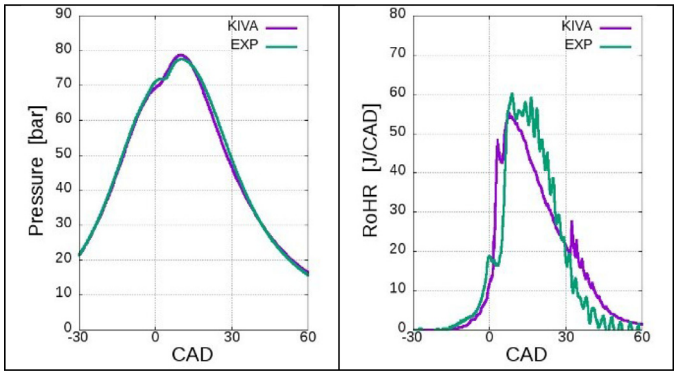

Fig. 10. Comparison between simulations and experiments: in-cylinder pressure (left) and Rate of Heat Release (right) for the case NG.

Figs. 10 and 11 report the comparison between simulations and experiments for CH_4 and NG cases. These figures show that, also for this new operating point, the code is able to correctly reproduce the combustion process, accurately predicting the in-cylinder pressure trace and the heat release curve. As expected, from the comparison between Figs. 10 and 11 it can be concluded that there is no

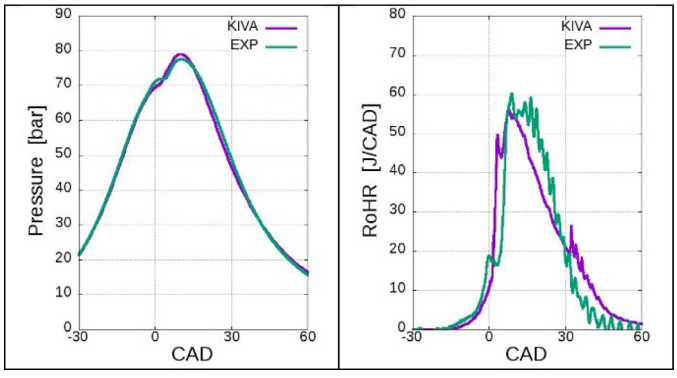

Fig. 11. Comparison between simulations and experiments: in-cylinder pressure (left) and Rate of Heat Release (right) for case CH_4.

noticeable difference when switching from NG (96% of methane) to pure methane.

Regarding biogas, Table 8 shows that the properties of the biogas blends are quite far from those of NG and CH_4, with particular reference to LHV and the Wobbe Index (WI). As well known, WI is a parameter that provides a measure for the interchangeability of gaseous fuel in SI engines: similar values of this parameter mean that AFR and laminar flame speed are comparable [36]. While the lower values of LHV for the biogas blends can be easily balanced by increasing the amount of premixed fuel, some care should be devoted to compensate the gap in terms of WI.

In a conventional SI engine, when switching from NG to biogas, or when changing biogas composition, a complex control system is generally required in order to maintain acceptable levels of engine regularity and performance. As an example, the experimental campaign reported in [37] on a single-cylinder SI engine fuelled with different blends of CH_4 and CO_2 (CH_4 from 50% to 100% in volume), shows that the growth of CO_2 percentage in the fuel makes BTE decrease and the combustion duration increase. In particular, at 8 Nm load, BTE decreases from 16.8% to 13.7% (−18%), as the fraction of CO_2 in the fuel increases from 0% to 40%.

A lower sensitivity to the low reactivity fuel composition is expected for dual fuel combustion. Figs. 12–17 show the results of combustion simulations for different biogas blends in the VM engine, operating in DF mode. In details, Fig. 12 shows the comparison between baseline (CH_4 case) and the cases with 3 different blends of biogas, namely BG50, BG65, and GB75 (ref. Table 8). Figs. 13–15 report the simulation results respectively for BG50, BG65 and BG75 obtained modifying the SOI (it has been advanced of 1, 2, 3 and 4 CAD for all the cases). Finally, Figs. 16 and 17 compare the results of all the simulations in terms of combustion efficiency, in-cylinder peak pressure and gross Indicated Mean Effective Pressure (IMEP*).

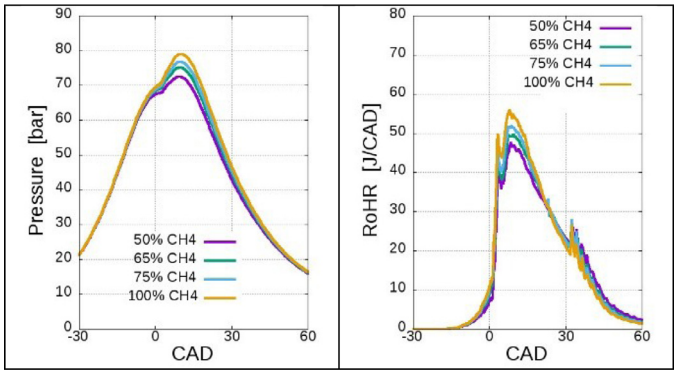

Fig. 12. Comparison between BG50 (50% CH_4), BG65 (65% CH_4), BG75 (75% CH_4) and 100% CH_4: in-cylinder pressure (left) and Rate of Heat Release (right).

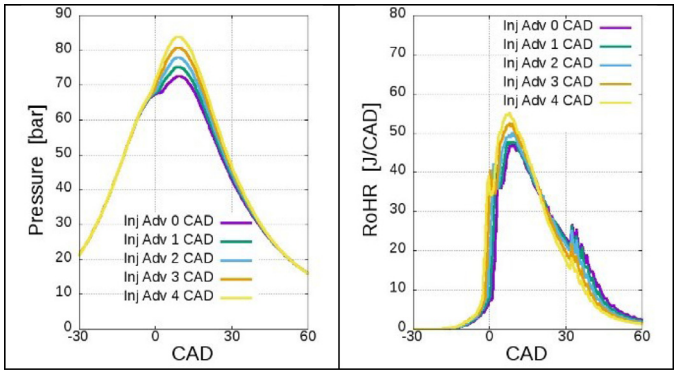

Fig. 13. Influence of Start of Injection on in-cylinder pressure (left) and Rate of Heat Release (right) for the case BG50.

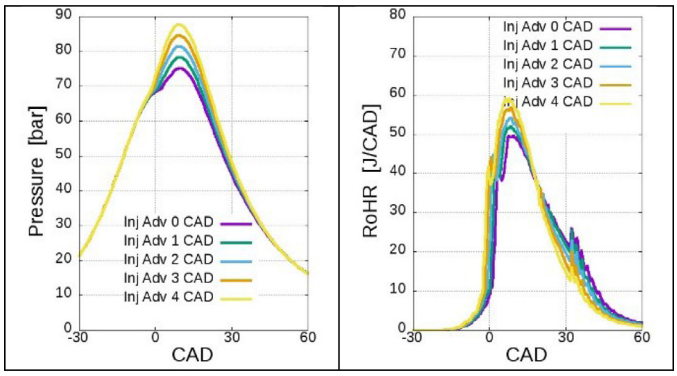

Fig. 14. Influence of Start of Injection on in-cylinder pressure (left) and Rate of Heat Release (right) for the case BG65.

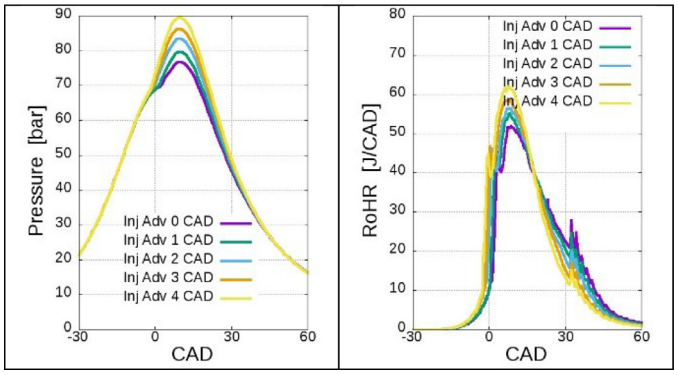

Fig. 15. Influence of Start of Injection on in-cylinder pressure (left) and Rate of Heat Release (right) for the case BG75.

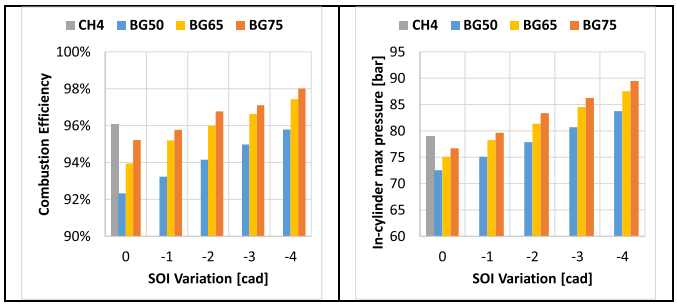

Fig. 16. Influence of Start of Injection on combustion efficiency (left) and in-cylinder max pressure (right).

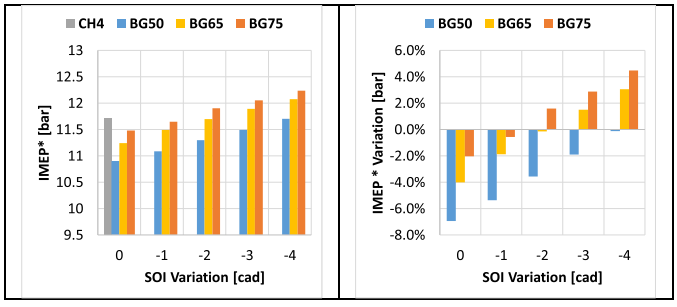

Fig. 17. Influence of Start of Injection on gross IMEP (left) and gross IMEP variation with reference to CH_4 case (right).

The last parameter is calculated as the pressure volume integral from −40 CA to +60 CA °ATDC, divided by the unit displacement. Fig. 12 clearly shows that, as the share of CO_2 increases in the biogas, the first part of the combustion process became slower; as a result, the

peak of both in-cylinder pressure and heat release rate decrease. The lower heat released in the first part of combustion is partially recovered in the second part but combustion efficiency remains slightly lower for all the biogas cases (about −4% for BG50, about −2% for BG65 and about −1% for BG75). For the same reasons, also IMEP* decreases (about −7% for BG50, about −4% for BG65 and about −2% for BG75).

These simulations demonstrate that engine efficiency and performance of the engine running in DF mode are weakly affected by the composition of biogas, even without a specific calibration of the engine control system. The only mandatory adjustment performed by the control system is on the biogas flow rate, that has to be increased when the CO_2 rises in the fuel mixture, in order to keep constant the fuel energy entering the cylinders. About this issue, it is observed that biogas composition can be easily monitored with reliable and cost-effective techniques, as reported in [38].

Moreover, the optimization of injection advance can easily compensate the small drop of BTE. As injection advance increases, combustion speed increases, improving both combustion efficiency and IMEP (see Figs. 13–15). For the BG75, an advance of 1 CAD is enough to reach the same combustion efficiency and IMEP* of the baseline, while for the BG65 and BG50 cases an advance of 2 and 4 CAD is needed. In conclusion, the CFD results show that the optimization of injection advance can completely cancel the dependence of the DF engine performance on the biogas composition.

7. Comparison with a conventional SI engine

In order to put the previous analysis into a context, as well as to assess the practical advantages of the proposed DF concept, a comparison is made with a commercial SI generator set, running on biogas, and delivering a maximum power strictly comparable to that of the RCCI engine. The main characteristics of the reference SI gen-set are listed in Table 9 [39].

The maximum power reported in Table 9 refers to a biogas blend composed by 65% in volume of methane and 35% in volume of CO_2. Therefore, also for the proposed DF CI engine, the above mentioned BG65 case with optimized SOI is considered. As discussed in the previous section, the optimum SOI advance permits to get the same combustion efficiency and IMEP* of the baseline NG engine.

From Table 9, it may be observed that the SI gen-set delivers a maximum power of 82.5 kW (load 100%) at the rated speed of 1500 rpm, with a fuel consumption of 36.8 Nm^3/h. In [39], fuel consumption is also provided for some partial loads (load 75, 50 and 25%).

Since a single operating condition (3000 rpm, 177 Nm / 55.5 kW) was investigated on the RCCI engine, some hypotheses are made in order to extrapolate the performances at the other loads. The following assumptions are made:

- engine speed is 3000 rpm, for all the loads;
- the same combustion and thermodynamic efficiency, measured for the baseline case, are maintained also in the other cases, thanks to a proper calibration of the engine (main calibration parameters: diesel fuel injection strategy, boost pressure);
- Friction Mean Effective Pressure (FMEP) is supposed to remain constant since the engine revolution speed is the same and the combustion mode is maintained.

Table 9
Main parameters of the reference SI gen-set running on biogas.

Manufacturer	HIMOINSA
Combustion Type	SI
Cylinders Lay-out	In-line
Number of cylinders	6
Air metering	Nat. asp.
Bore x Stroke [mm]	130×150
Displacement [L]	11.946
Compression Ratio	12:1
Injection system	PFI
Rated rpm@50 Hz	1500
Max. Power at rated rpm [kW]	82.5
Max. BMEP at rated rpm [bar]	5.5
Fuel consumption at Max. Power, rated rpm [Nm^3/h]	36.8
BSFC at Max. Power, rated rpm [g/kWh]	513.8
Max. Specific Power, rated rpm [kW/L]	6.9

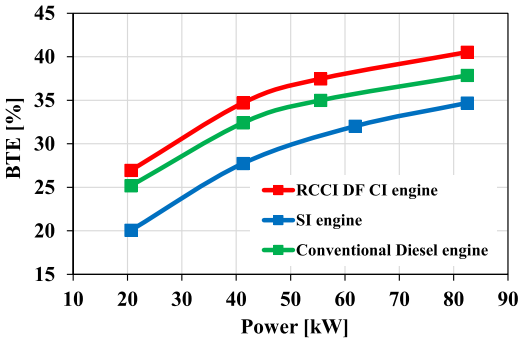

Fig. 18. Comparison among the RCCI DF engine, the SI engine and the conventional diesel engine.

The comparison between the two engines is presented in Fig. 18. As expected, the higher thermodynamic and pumping efficiency of the CI engine guarantees a higher BTE over the whole operating range. The maximum improvement (34%) is at low load, due to the high throttling losses of the SI engine. At the operating point of maximum interest (55 kW), the fuel saving offered by RCCI is about 21%.

Another advantage of the RCCI engine, that can be deduced from the comparison between Tables 5 and 9, is the much more compact dimensions (4 cylinders vs. 6, bore 94 mm versus 130 mm, et cetera). Last but not the least, the number of components of the "donor" engine that must be modified for running on biogas is smaller: as an example, the RCCI engine can work with the original pistons, without varying the compression ratio.

For the sake of completeness, Fig. 18 also reports the trend of BTE as a function of the power delivered for the conventional Diesel engine. As expected, the donor Diesel engine presents a higher efficiency compared to the SI engine.

8. Economic analysis

As previously demonstrated, the proposed DF engine can be conveniently used as the energy source of a micro-cogeneration system, running on biogas. For the study case presented in Section 2, it is also convenient to have a self-production of biogas, installing a facility in the farm. The same biogas can be used to replace the NG burning in the crop drying system, making the farm completely independent on the external fuel supply and reducing the cost of energy purchasing. The economic impact of the installation of the biogas production facility, combined with the micro-cogeneration system is analyzed in this section.

In order to carry out its production processes, the farm has an annual cost for energy of about 200,000 €, split as it follows:

- 55,000 € for electrical energy (current average specific cost equal to 0.18 €/kWh, in Italy);
- 140,000 € for NG (current average specific cost equal to 0.7 €/Nm^3, in Italy).

Table 10
Annual amounts of cattle manure and crops employed for biogas production.

	Quantity [ton/year]	Biogas production [Nm^3/year]
Cattle manure	576	173,000
Crops	87	43,250

- 4100 € for Diesel fuel (current average specific cost equal to 1 €/litre, in Italy).

As it can be deduced from the analysis presented in Section 2 and considering that the dryer has an efficiency of 60%, the thermal energy demand for the crop drying process is 1700,000 kWh, corresponding to a consumption of 181,000 Nm^3 of NG, for an annual cost of 126,000 €.

The biogas can be produced by an anaerobic digester, mainly fed with cattle manure and, to a lesser extent, with crops. The specific production of biogas from cattle manure is about 300 Nm^3/ton_{ss}, while from crops is about 500 Nm^3/ton_{ss} [40]. The manure production of the farm is over 1800 ton/year, supposing an average dejection for each animal of about 10 ton/year. However, only a limited share of this manure can be used for biogas. Employing also crops in the digester, the thermal power demand of the dryer is reduced. In particular, the thermal power demand decreases from 530 kW to 502 kW, maintaining the working period of 200 days and 16 h/day. In this way, the farm can become completely independent on the NG supply. Table 10 reports the annual amounts of cattle manure and crops addressed to the biogas plant and the corresponding biogas production.

It is considered that the electrical energy demand of the farm increases by 12% because of the biogas plant electrical needs.

As far as the micro-cogeneration system is concerned, it guarantees a maximum electrical power of 48 kW (electrical power absorbed by the ancillaries: 2 kW), while the maximum rejected thermal power is about 55 kW. The 25% of the heat produced by the system is used for the anaerobic digestion process.

The new electrical power demand profiles are depicted in Fig. 19, while the new thermal power profiles are shown in Figs. 20 and 21.

Thanks to the micro-cogeneration, the purchase of electrical energy from the public grid is reduced by 50% in a year (from 308,000 kWh to 152,000 kWh), with a saving of 22 450 €/year.

In the crop drying period, the micro-cogeneration also provides 10% of the required thermal energy. Although the purchase of Diesel fuel is more than doubled (from 4200 €/year to 10,200 €/year), it should be noted that the expense for NG, previously equal to 140,000 €/year, is completely eliminated, thanks to the production of biogas.

A crop quota is no longer available for sale, with a loss of about 7500 €/year.

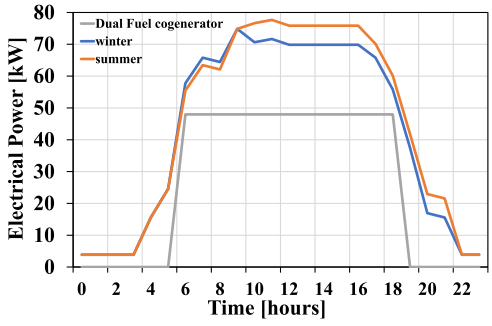

Fig. 19. Electrical power demand of the farm with biogas production plant (blue and orange lines) and electrical power provided by micro-cogeneration (grey line) (For interpretation of the references to color in this figure legend, the reader is referred to the web version of this article.).

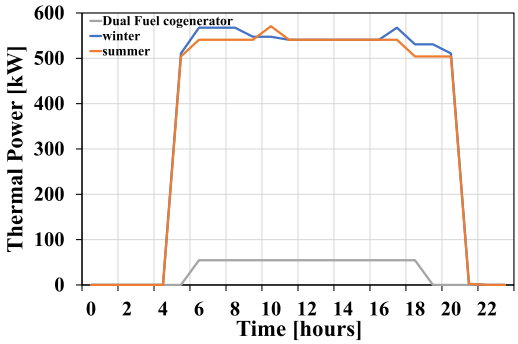

Fig. 20. Thermal power demand of the farm with biogas production plant (blue and orange lines) and thermal power provided by micro-cogeneration (grey line) (For interpretation of the references to color in this figure legend, the reader is referred to the web version of this article.).

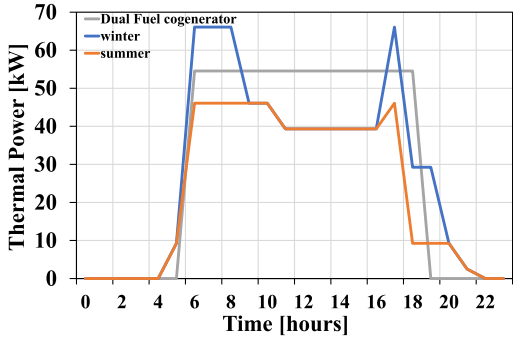

Fig. 21. Thermal power demand of the farm with biogas production plant (blue and orange lines), without crop drying process, and thermal power provided by micro-cogeneration (grey line) (For interpretation of the references to color in this figure legend, the reader is referred to the web version of this article.).

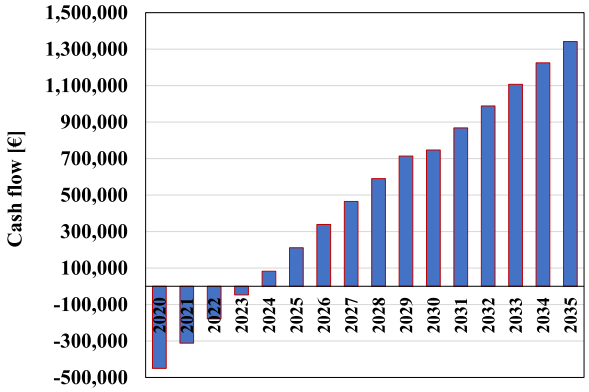

Fig. 22. Net actual value.

Moreover, the maintenance cost of the biogas plant, as well as of the micro-cogeneration system is taken into account. It corresponds to about 13,000 €/year (ordinary maintenance: 200 €/kW_e, extraordinary maintenance 50 €/kW_e).

As a final result of the investment, the cash flow of the farm is 136,000 €/year.

The entire plant (biogas plant and micro-cogeneration system) requires an investment of 450,000 €, including the connection to the public electrical grid and the authorization procedures. The resulting cash flow, considering a precautionary discount rate of 1%, enables a return of the same investment in 5.3 years, leading to a net actual value, calculated over 10 years, of € 750,000. Moreover, considering a complete substitution of the micro-cogeneration system and of some components of the biogas plant after 10 years, for an expense of about € 100,000, the net actual value after 15 years will be € 1340,000 (see Fig. 22).

9. Conclusions

The present paper describes the results of an experimental and numerical study carried out on a 4-cylinder, Common Rail, 2.8 L turbocharged Diesel engine for automotive applications, Euro IV compliant. The aim of the activity is to implement and optimize a Reactivity Controlled Compression Ignition Dual Fuel biogas-diesel combustion concept in order to adopt such an engine in a micro-cogeneration system. In order to maximize the environmental advantages, the biogas is supposed to be produced in situ.

The study is carried out considering the specific needs of a typical medium sized agro-zootechnical company, located in Italy, producing milk and cheese and selling forage. First of all, the thermal and electrical demands of the farm are analysed in detail, determining the electric power rate of the micro-cogeneration system: 50 kW at 3000 rpm.

The advantages of the proposed dual fuel CI engine, in comparison to a conventional SI engine delivering the same power and running on biogas are:

- ≈20% increase of BTE, due to the higher efficiency of the thermodynamic cycle (higher compression ratio), lower thermal and pumping losses;
- ≈20% reduction of CO_2 emissions, due to the lower biogas consumption;
- lower sensitivity to biogas composition, simpler engine control system;
- lower number of components that must be modified for transforming a Diesel engine into a biogas engine (the combustion chamber can remain the same, no need of replacing the pistons and installing the ignition system);
- more compact overall dimensions.

In comparison to a conventional diesel engine, the new dual fuel unit running on self-produced biogas can cut the cost of the fuel, and considerably reduce the soot emissions. The only drawback is the higher emissions of HC and CO, requiring the installation of a specific oxidation catalyst.

Finally, for the considered study case, the micro-cogeneration associated to an anaerobic digester for the production of biogas can provide a net actual value, after 15 years of € 1340,000.

Declaration of Competing Interest

None.

Acknowledgments

This research did not receive any specific grant from funding agencies in the public, commercial, or not-for-profit sectors.

Supplementary materials

Supplementary material associated with this article can be found in the online version at doi:10.1016/j.ijft.2021.100093.

References

[1] B. Egilegor, H. Jouhara, J. Zuazua, F. Al-Mansour, K. Plesnik, L. Montorsi, L. Manzini, ETEKINA: analysis of the potential for waste heat recovery in three sectors: aluminium low pressure die casting, steel sector and ceramic tiles manufacturing sector, Int. J. Thermofluids 1 (2020) 100002.
[2] H. Jouhara, A. Żabnieńska-Góra, N. Khordehgah, D. Ahmad, T. Lipinski, Latent thermal energy storage technologies and applications: a review, Int. J. Thermofluids 5 (2020) 100039.
[3] J.J. Fierro, A. Escudero-Atehortua, C. Nieto-Londoño, M. Giraldo, H. Jouhara, L.C. Wrobel, Evaluation of waste heat recovery technologies for the cement industry, Int. J. Thermofluids 7 (2020) 100040.
[4] ... & H. Jouhara, A. Żabnieńska-Góra, N. Khordehgah, Q. Doraghi, L. Ahmad, L. Norman, S. Dai, Thermoelectric generator (TEG) technologies and applications, Int. J. Thermofluids (2021) 100063.
[5] S.H. Yoon, C.S. Lee, Experimental investigation on the combustion and exhaust emission characteristics of biogas–biodiesel dual-fuel combustion in a CI engine, Fuel Process. Technol. 92 (5) (2011) 992–1000.
[6] D. Splitter, R. Hanson, S. Kokjohn, R.D. Reitz, Reactivity controlled compression ignition (RCCI) heavy-duty engine operation at mid-and high-loads with conventional and alternative fuels (No. 2011-01-0363), SAE Tech. Paper (2011).
[7] S. Padala, C. Woo, S. Kook, E.R. Hawkes, Ethanol utilisation in a diesel engine using dual-fuelling technology, Fuel 109 (2013) 597–607.
[8] Y. Zhang, I. Sagalovich, W. De Ojeda, A. Ickes, T. Wallner, D.D. Wickman, Development of dual-fuel low temperature combustion strategy in a multi-cylinder heavy-duty compression ignition engine using conventional and alternative fuels, SAE Int. J. Engin. 6 (3) (2013) 1481–1489.
[9] Y. Li, M. Jia, Y. Liu, M. Xie, Numerical study on the combustion and emission characteristics of a methanol/diesel reactivity controlled compression ignition (RCCI) engine, Appl. Energy 106 (2013) 184–197.
[10] J. Liu, F. Yang, H. Wang, M. Ouyang, Numerical study of hydrogen addition to DME/CH4 dual fuel RCCI engine, Int. J. Hydrog. Energy 37 (10) (2012) 8688–8697.
[11] D.E. Nieman, A.B. Dempsey, R.D. Reitz, Heavy-duty RCCI operation using natural gas and diesel, SAE Int. J. Eng. 5 (2) (2012) 270–285.
[12] S. Curran, R. Hanson, R. Wagner, Effect of E85 on RCCI performance and emissions on a multi-cylinder light-duty diesel engine. No. 2012-01-0376. SAE Tech. Paper, 2012.
[13] R.G. Papagiannakis, C.D. Rakopoulos, D.T. Hountalas, D.C. Rakopoulos, Emission characteristics of high speed, dual fuel, compression ignition engine operating in a wide range of natural gas/diesel fuel proportions, Fuel 89 (7) (2010) 1397–1406.
[14] S. Molina, A. García, J.M. Pastor, E. Belarte, I. Balloul, Operating range extension of RCCI combustion concept from low to full load in a heavy-duty engine, Appl. Energy 143 (2015) 211–227.
[15] H. Liu, Q. Tang, Z. Yang, X. Ran, C. Geng, B. Chen, M. Yao, A comparative study on partially premixed combustion (PPC) and reactivity controlled compression ignition (RCCI) in an optical engine, Proc. Combust. Inst. 37 (4) (2019) 4759–4766.
[16] Q. Tang, H. Liu, M. Li, C. Geng, M. Yao, Multiple optical diagnostics on effect of fuel stratification degree on reactivity controlled compression ignition, Fuel 202 (2017) 688–698.
[17] L. Tong, H. Wang, Z. Zheng, R. Reitz, M. Yao, Experimental study of RCCI combustion and load extension in a compression ignition engine fueled with gasoline and PODE, Fuel 181 (2016) 878–886.
[18] Z. Zheng, M. Xia, H. Liu, X. Wang, M. Yao, Experimental study on combustion and emissions of dual fuel RCCI mode fueled with biodiesel/n-butanol, biodiesel/2, 5-dimethylfuran and biodiesel/ethanol, Energy 148 (2018) 824–838.
[19] Y. Cui, Z. Zheng, M. Wen, Q. Tang, C. Geng, Q. Wang, M. Yao, Optical diagnostics on the effects of reverse reactivity stratification on the flame development in dual-fuel combustion, Fuel 287 (2021) 119500.
[20] E. Mattarelli, C. Rinaldini, T. Savioli, F. Scrignoli, Optimization of a high-speed dual-fuel (Natural Gas-Diesel) compression ignition engine for gen-sets, SAE Int. J. Eng. 14 (3) (2021), doi: 10.4271/03-14-03-0022.
[21] G. Grazzini, C. Balocco, D. Paganini, “Rilevazione in campo consumi elettrici e termici di aziende agricole campione” (Progetto MODERNO) 2021
[22] E. Ernesto Tabacco, G. Borreani, L. Comino, A. Revello (Edizioni L'Informatore Agrario)
[23] M.C. Cameretti, R. De Robbio, R. Tuccillo, Performance improvement and emission control of a dual fuel operated diesel engine. No. 2017-24-0066 SAE Tech. Paper (2017).
[24] M. Milani, L. Montorsi, M. Venturelli, A combined numerical approach for the thermal analysis of a piston water pump, Int. J. Thermofluids 7 (2020) 100050.
[25] M. Milani, L. Montorsi, G. Storchi, M. Venturelli, D. Angeli, A. Leonforte, A. Sorrentino, Experimental and numerical analysis of a liquid aluminium injector for an Al-H_2O based hydrogen production system, Int. J. Thermofluids 7 (2020) 100018.
[26] A.A. Amsden, “KIVA-3V: a block-structured KIVA program for engines with vertical or canted valves,” LA- 13313-MS, 1997.
[27] J. Gustavsson, V.I. Golovitchev, Spray combustion simulation based on detailed chemistry approach for diesel fuel surrogate model, SAE Tech. Paper (2003) 2003-01- 1848, doi: 10.4271/2003-01-1848.
[28] V.I. Golovitchev, C.A. Rinaldini, L. Montorsi, A. Rosetti, CFD combustion and emission formation modeling for a HSDI diesel engine using detailed chemistry, in: Proceedings of the (2006) ASME ICEF, 2006, p. 10. ISBN: 0791837920; 978-079183792-4.
[29] V.I. Golovitchev, N. Nordin, R. Jarnicki, J. Chomiak, 3-D diesel spray simulations using a new detailed chemistry turbulent combustion model, SAE Tech. Paper (2000) 2000-01-1891, doi: 10.4271/2000-01-1891.
[30] R. Ehleskog, V. Golovitchev, I. Denbratt, S. Andersson, C.A. Rinaldini, Experimental and numerical investigation of split injections at low load in an hddi diesel engine equipped with a piezo injector, SAE Tech. Papers (2006), doi: 10.4271/2006-01-3433.
[31] V.I. Golovitchev, A. Imren, Development of dual fuel combustion models for direct injected heavy duty diesel engines, Diesel Fuels: Characteristics, Performances and Environmental Impacts, Nova Pusblisher, 2013 ISBN: 978-1-62618-867-9.
[32] E. Mattarelli, C.A. Rinaldini, V.I. Golovitchev, CFD-3D analysis of a light duty dual fuel (Diesel/Natural Gas) combustion engine, Energy Procedia. 45 (2014) 929–937.

[33] C.A. Rinaldini, E. Mattarelli, V.I. Golovitchev, Potential of the miller cycle on a HSDI diesel automotive engine, Appl. Energy 112 (2013) 102–119.
[34] C.A. Rinaldini, G. Allesina, S. Pedrazzi, E. Mattarelli, P. Tartarini, Modeling and optimization of industrial internal combustion engines running on diesel/syngas blends, Energy Convers. Manag. 182 (2019) 89–94.
[35] G. Cantore, E. Mattarelli, C.A. Rinaldini, T. Savioli, F. Scrignoli, Numerical optimization of the injection strategy on a light duty diesel engine operating in dual fuel (CNG/Diesel) mode, Int. J. Heat Technol. 37 (3) (2019) 682–688.
[36] Jacob, Interchangeability of gaseous fuels-the importance of the wobbe-index, SAE Trans. (1986) 962–972.
[37] J. Liu, CE. Dumitrescu, Numerical investigation of methane number and wobbe index effects in lean-burn natural gas spark-ignition combustion, Energy Fuels 33 (5) (2019) 4564–4574.
[38] C. Rahmouni, M. Tazerout, O. Le Corre, A method to determine biogas composition for combustion control, SAE Trans. (2002) 700–709.
[39] HIMOINSA, “HIMOINSA HGE-95 T5 BIO 92 kVA standby generator set open skid datasheet”, accessed 2020, https://www.himoinsa.com/eng/electric-generators/325/generator-set−92kva−open-skid.html
[40] S. Castelli, “Biomasse ed energia” (Maggiori Editore)